BOR DERGİSİ
JOURNAL OF BORON
https://dergipark.org.tr/boron

Boron-doped WO_3 thin films prepared by thermionic vacuum arc technique: The structural, surface, and optical properties

Saliha Elmas [1,*]

[1]*Kocaeli Health and Technology University, European Vocational School, Medical Imaging Techniques Program, Kocaeli, 41190, Türkiye*

ARTICLE INFO

Article history:
Received December 20, 2023
Accepted March 30, 2024
Available online June 28, 2024

Research Article

DOI: 10.30728/boron.1407455

Keywords:
Boron-doped WO_3
Dielectric constant
Optical band gap
Roughness
Surface properties

ABSTRACT

Improvement in the physical properties of WO_3 thin films is of great interest among researchers. In this work, boron as a dopant was selected to enhance the physical characteristics of the WO_3 thin films on glass and silicon wafer substrates. To achieve this aim, a plasma-based, well-known thermionic vacuum arc (TVA) technique was utilized to prepare the films with varying boron percent, followed by structural, optical, and microscopic characterization. The roughness of the films directly depends on the boron amount and nature of the substrate. The structural measurement proved the formation of WO_3 phases on both substrates. An increase in the dopant amount caused a shift in the dominant peak in the X-ray diffraction patterns. The crystallite sizes of the films varied in the range of 14-49 nm. According to the optical results, the optical band gaps (E_g) of the WO_3:B (1%) and WO_3:B (3%) films were obtained as 3.23 and 3.25 eV, respectively. The increase in the boron amount led to an increase in the packing density of the films. This behavior was not related to substrate properties. These results suggest a direct relationship between crystallite size and lower optical loss function.

1. Introduction

Due to the quality, high interest, and wide application area, the materials of oxides, nitrides, and carbides gained great attention from both scientific and industrial sides. Among those, oxides are a material group with individual and special characteristics. So far, various classes of oxide materials have been discovered, synthesized, and coated by different chemical and physical-based techniques [1-4]. In this class, tungsten trioxide (WO_3) is of great interest due to its chemical excellence, mechanical stability, physical stability, and so on [5,6]. The mentioned properties lead to extending the application area of the material. Since the discovery of the oxide material, several methods have been used for synthesizing and coating upon various substrates. Despite the advantages mentioned above, some challenges still cause the restricted use of WO_3 in all applications. To overcome this problem, some routes, such as doping, multi-layer structures, and composite with other materials, are recommended and carried out to improve the WO_3 structure [4,7]. Researchers have successfully doped WO_3 thin films with various elements such as Al [5], Mn [7], Fe [8], C [9], or oxides i.e. CuO [10], MoO_3 [11]. In this research, boron is selected as a dopant to improve the properties of the WO_3 thin film. Overall, thin films have been coated with the plasma-based thermionic vacuum arc (TVA) technique in the high vacuum regime. Then, the suitable devices measure and evaluate the boron-doped WO_3 (WO_3:B) thin films' physical properties.

Alsaad et al. [12] concentrated on the optical and optoelectronic properties of boron-doped ZnO thin films prepared by the sol-gel method. The group proposed a new mathematical equation between thickness and optical band gap for amorphous or crystalline structures. A reverse relationship between boron concentration and optical band gap was proposed. Also, a reverse correlation between Urbach and boron dopant amount was found. Eskalen et al. [13] studied radiation shielding characteristics of wurtzite-structured ZnO:B thin films prepared using a spray pyrolysis method. The researchers report deformation in the structure and worsened in the hexagonal rods respecting the surface images due to incorporating a boron dopant in the host structure. Additionally, a direct dependency between boron dopant and linear attenuation coefficient, mass attenuation coefficient, half value layer, one-tenth value layer, and mean free path results was pronounced. Wong and Lai [14] published a work investigating the temperature dependency of boron-doped ZnO thin films produced via the sputtering technique. Due to the boron activation, the results confirmed the best electrical properties at 400°C in the ZnO:B thin films. More than the boron dopant amount, according to the work, the best optical, morphological, and structural properties of the films were related to deposition temperature.

*Corresponding author: saliha.elmas@kocaelisaglik.edu.tr

This research's main target is introducing a new and quick pathway for forming WO_3:B thin films based on utilizing plasma and vacuum-based techniques. In this context, the relation between coating parameters and physical properties is described in detail.

2. Materials and Methods

2.1. Materials

The WO_3 (99.5% purity) and B powders (99.5% purity) were purchased from the Nanografi (Türkiye) company and Alfa Aesar (USA), respectively. Acetone, isopropanol, and Si substrates (N-type p-doped (111) orientation) were from ISOLAB (Germany), Detsan (Türkiye) and MTI cooperation (USA), respectively.

2.2. Methods

The WO_3 material was doped 1% and 3% in weight. The prepared pellets' diameter and thickness were 1 cm and 1 mm, respectively. The glass and Silicon (Si) wafers were used for substrates. The substrates were ultrasonically cleaned by deionized water (50°C), acetone (30°C) and isopropanol (30°C) for 5 minutes to remove the particles on the substrates, respectively. The glass and Si substrates were cleaned according to the procedure seen in Figure 1. The Si substrate is p-doped with (111) orientation.

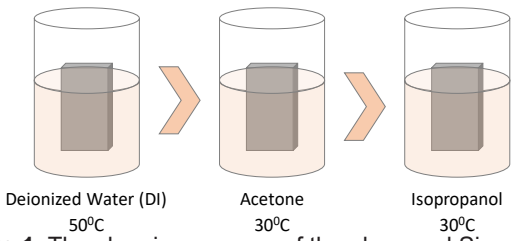

Figure 1. The cleaning process of the glass and Si substsrates.

The coating process was performed using a plasma-based technique that well-known as TVA in a high vacuum regime. Firstly, the cleaned substrates were placed in the chamber upon the substrate holder. Then the substrate holder is fixed on the anode and kept at a constant distance from the anode during the coating. The anode section is a spoon-like tungsten (W) or Molybdenum (Mo)-included material for holding the coated material on the substrate. In our case, the boron-doped WO_3 powder as a pellet was poured inside the anode gently. The vacuum chamber was closed and the evacuation process started. Initially, the rotary pump and the turbo-molecular pump started. This process was continued until the pressure value achieved base pressure means $7x10^{-6}$ Torr. All processes such as evacuation, coating, amount of current, and voltage applied were monitored and controlled by various and suitably mounted devices. The coating process was started by applying AC and DC currents to the cathode and anode parts [1]. The cathode is constructed of tungsten wire surrounded by the Wehnelt cylinder and serves as an electron gun. After applying the current and voltage to the cathode, the tungsten wire is thermally heated, leading to electron emission. The emitted electrons moved toward the anode while using the Wehnelt the random movement of these electrons was avoided [2]. The collisions between the electrons and pelletized WO_3:B powders cause energy transfer, then a change in the phase of powders to liquid and so gas phases. This procedure continues after reaching a stable plasma of WO_3:B. This plasma was moved onto the substrate holder and deposited layer by layer on the cleaned substrates. The significant parameters during the coating are listed in Table 1.

Table 1. The effective TVA parameters during the coating process.

Parameters	WO_3:B	
	1%	3%
Discharge current (A)	0.30	0.25
Deposition time (s)	60	180
Working pressure (Torr)	$1.8x10^{-4}$	$2.04x10^{-4}$
Applied voltage (V)	200	200
Filament current (A)	18.7	18.2

Thin films were analyzed by Ambios Q-scope Atomic Force Microscope (AFM) in non-contact mode using the Scan Atomic V 5.1.0 SPM control software at room temperature. Compositional characterization of WO_3:B thin films was analyzed with, using Al source, X-ray photoelectron spectroscopy (XPS, Thermo Scientific K-Alpha, USA). The device works in a dual source light source utilizing ultra-low energy electron beam and Al Kα micro-focused condition. The structural properties of the films were measured through a X-ray diffraction (XRD, Malvern Panalytical Empyrean, UK). The optical features of the thin films were characterized using UV-VIS spectrophotometry (Unico Dual Beam, USA) and Filmetrics F20 devices. The UV-Vis spectrophotometry and Filmetrics were performed in 200-1100 nm and 400-1000 nm wavelength ranges, respectively. Both optical devices work at room temperature. The surface properties of the produced films were investigated with scanning electron microscopy (SEM, Zeiss Supra 40VP, Germany).

3. Results and Discussion

The three-dimensional (3D) images and crystallite distribution of the particles upon the surface of the boron-doped WO_3 thin films are shown in Figure 2. Using AFM, roughness, crystallite sizes, and symmetric distribution of the crystals upon the surface after the coating was revealed, as seen in Table 2. According to the measurement results, an increase in the boron amount is not affected by the roughness values, while an increase in the boron percent leads to a decrease in the roughness. So, the roughness value is directly related to substrate and boron amount.

The skewness is an indication of the symmetric distribution of particles on the surface [2]. In both

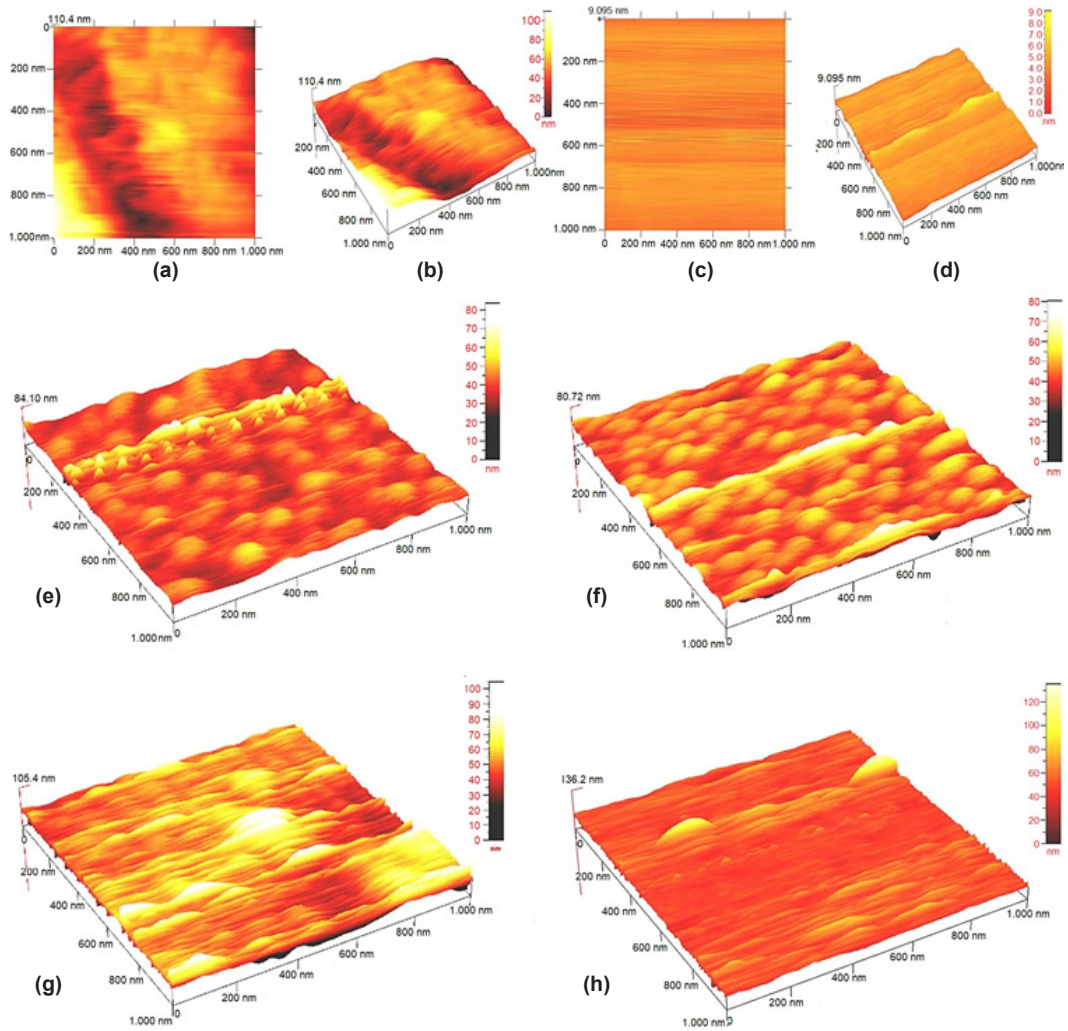

Figure 2. The AFM images of the a, b) bare glass substrate, c, d) bare Si wafer substrate, e) WO_3:B/glass (1%), f) WO_3:B (3%)/glass, g) WO_3:B (1%)/Si, h) WO_3:B (3%)/Si.

Table 2. The surface results obtained using the AFM device.

	RMS (nm)	Skewness (Ssk)	Kurtosis (Skr)
Bare glass substrate	13.1	0.97	0.74
Bare Si wafer substrate	0.33	3.78	40.88
WO_3:B (1%)/glass	5.01	0.08	4.1
WO_3:B (1%)/Si	9,39	0.16	1.96
WO_3:B (3%)/glass	5.13	0.24	3.12
WO_3:B (3%)/Si	6,48	0.70	11.56

cases, the highest symmetric distribution is measured at the films coated upon the glass substrate. This characteristic is not dependent on boron dopant percent.

The FESEM images of the coated films are shown in Figure 3. All images are portrayed in the 50,000X resolution. Regarding the images, there are no cracks on the surface. This feature is not related to the boron amount and substrate. Increasing the boron amount in the host material causes some agglomeration on the surface. The surfaces are compact and dense without pinholes. This characteristic shows the eligibility of the films for use in dye-synthesized solar cells [12]. The grains on the surface are spherical ball-like configurations that do not depend on the boron and substrate nature.

The micro-structural properties of the prepared films are performed and listed in Table 3. In the XRD patterns (Figure 4), WO_3 and B_2O_3 peaks demonstrate the polycrystalline nature of the prepared films. The result is not related to the structure of the substrate. According to the measurement, there are shifts in the WO_3 peaks, which show stress during the coating because of the boron dopant. This stress originated from adding dopant into the host structure, as reported by other researchers [1] and is responsible for the shift in the emerged peaks.

Regarding the patterns, the structure has no impurity, other phases, or bond between W and B. Significantly, in this case, the high-intensity peak is directly related to the amount of dopant. In the low dopant (1%) of the films, the high-intensity peak was WO_3 with (004) diffraction plane, while in the high dopant (3%), the highest peak was WO_3 with (222) diffraction plane.

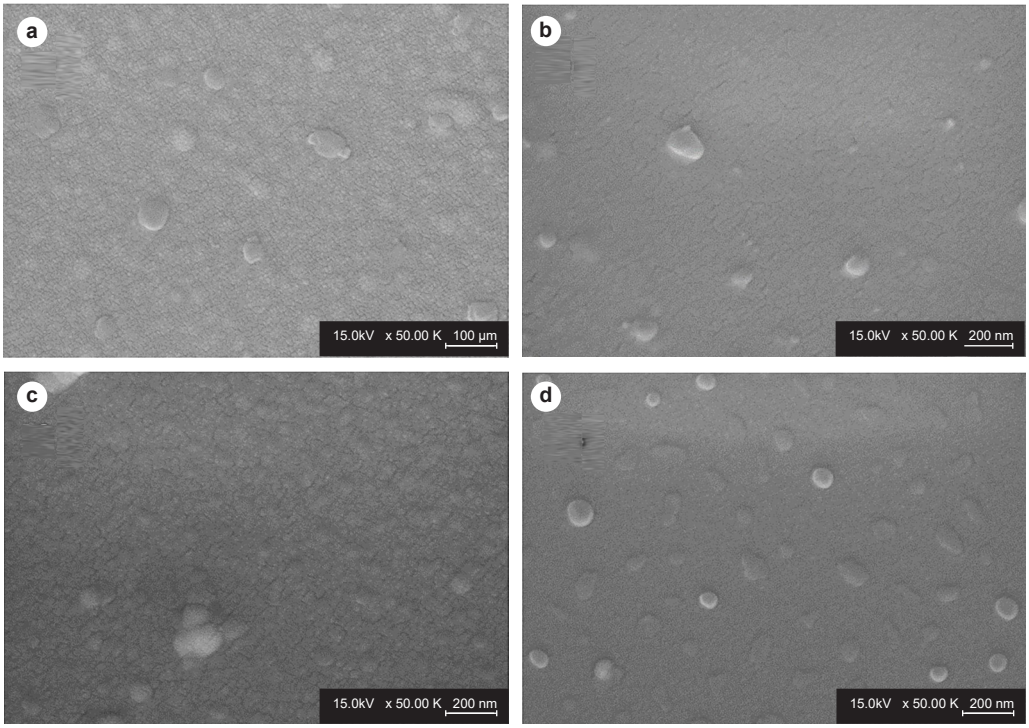

Figure 3. The FE-SEM images of the a) WO_3: B (1%)/glass, b) WO_3: B (1%)/Si, c) WO_3: B (3%)/glass, d) WO_3: B (3%)/Si (Scale bar: 1µm).

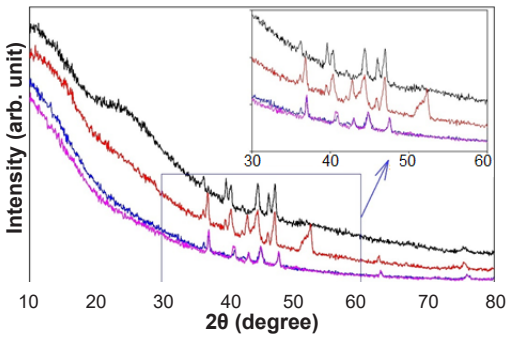

Figure 4. The XRD pattern of the Boron-doped WO_3 on glass and Si substrates, WO_3:B/glass (1%, black line), WO_3:B/Si (1%, red line), WO_3:B/glass (3%, blue line), and WO_3:B/Si (3%, pink line).

Therefore, increasing the boron amount causes a change in the WO_3 diffraction plane. This issue is not related to the nature of the utilized substrate. All emerging peaks show monoclinic WO_3 crystal structure and are compatible with ICDD card No: 43-1035 [2].

Using the patterns, for both substrates, the crystallite size (CS) of the films is calculated by the well-known Scherrer formula (Eq. 1) [3,4], where, the λ (=1.5406 Á), FWHM, and θ are the X-ray wavelength, full width at half maximum of a peak, and Bragg diffraction angle, respectively.

$$CS = \frac{0.94\,\lambda}{FWHM\cos\theta} \quad (1)$$

Respecting the results, the minimum and maximum grain sizes of the thin films coated on both substrates were altered between 14 and 49 nm, respectively. These results proved the eligibility of the TVA in the formation and growth of nanometer crystals on the various substrates. Despite the lack of thermal treatment application to produce the thin films, these values are comparable and, in some cases, smaller than the other coated WO_3 films in the literature [5-9].

Utilizing the above results, the dislocation density (δ) and microstrain (ε) residue in the coated thin films are calculated by Eq. (2) and (3) [4,10].

$$\delta = (CS)^{-2} \quad (2)$$

$$\varepsilon = \frac{FWHM\cos\theta}{4} \quad (3)$$

Considering the coating method, there are defects in the prepared thin film. In this situation, the defects during the coating process via TVA were computed and listed in the table. Also, the lattice strain (LS) due to pressure change during the coating, as well as the dopant effect, is evaluated by Eq. (4) [10-12].

$$LS = \frac{FWHM}{4\tan\theta} \quad (4)$$

These values are outlined in Table 3. The stress and strain values during the coating as well as dopant effects are comparable with other reported research in literature [1,6,13].

According to the calculated results, an increase in the boron dopant causes a reduction in the intensity of the maximum XRD peaks, replacement of (004) with (222) plane, and sharpening in the maximum emerged peak [1,7,14]. Amongst the various reasons for emerging the secondary phase, the existence of B_2O_3 in this structure is concluded owing to the large difference in

Table 3. The results of XRD measurement for the coated films on both substrates.

	Peak 2θ (˚)	Diffraction plane (hkl)	Phase	Crystal size (nm)	Dislocation density (δ) $(nm)^{-2}$	Microstrain (ε)	Lattice strain (LS)	ICCD card
WO_3:B/glass (1%)	36.15	122	WO_3	31	1.04×10^{-3}	7.44×10^{-2}	0.24	72-0199
	39.60	240	WO_3	48	4.34×10^{-4}	4.91×10^{-2}	0.14	72-0199
	40.33	021 103	WO_3 B_2O_3	27	1.37×10^{-3}	8.57×10^{-2}	0.25	98-008-9092 72-0199
	44.39	320	WO_3	23	1.89×10^{-3}	9.66×10^{-2}	0.26	72-0199
	46.01	123	WO_3	49	4.16×10^{-4}	4.80×10^{-2}	0.12	72-0199
	46.97	112 004	B_2O_3 WO_3	39	6.57×10^{-4}	5.98×10^{-2}	0.15	98-005-1575 72-0199
WO_3:B/Si (1%)	36.83	222	WO_3	37	7.30×10^{-4}	6.19×10^{-2}	0.20	43-1035
	40.32	103	B_2O_3	27	1.37×10^{-3}	8.57×10^{-2}	0.25	43-1035
	42.80	133	WO_3	23	1.89×10^{-3}	9.71×10^{-2}	0.27	43-1035
	44.34	320	WO_3	38	6.93×10^{-4}	6.04×10^{-2}	0.16	43-1035
	45.88	123	WO_3	38	6.93×10^{-4}	6.00×10^{-2}	0.15	43-1035
	46.93	112 004	B_2O_3 WO_3	39	6.57×10^{-4}	5.98×10^{-2}	0.15	98-007-4774 43-1035
	52.31	420	WO_3	50	4.00×10^{-4}	4.68×10^{-2}	0.11	43-1035
	62.58	143	WO_3	34	8.65×10^{-4}	6.68×10^{-2}	0.13	43-1035
	75.49	030	B_2O_3	18	3.09×10^{-3}	1.24×10^{-1}	0.20	98-007-4774
WO_3:B/glass (3%)	36.94	222	WO_3	48	4.34×10^{-4}	4.95×10^{-2}	0.16	43-1035
	40.87	103	B_2O_3	31	1.04×10^{-3}	7.33×10^{-2}	0.21	98-008-0829
	42.86	133	WO_3	15	4.44×10^{-3}	1.46×10^{-1}	0.40	43-1035
	44.81	123	WO_3	32	9.77×10^{-4}	7.23×10^{-2}	0.19	43-1035
	47.51	312	WO_3	39	6.57×10^{-4}	5.97×10^{-2}	0.15	43-1035
	62.88	143	WO_3	34	8.65×10^{-4}	6.67×10^{-2}	0.13	43-1035
	75.97	030	B_2O_3	14	5.10×10^{-3}	1.64×10^{-1}	0.27	96-151-0795
WO_3:B/Si (3%)	36.99	222	WO_3	48	4.34×10^{-4}	4.95×10^{-2}	0.16	43-1035
	40.77	103	B_2O_3	23	1.89×10^{-3}	9.78×10^{-2}	0.28	98-000-8217
	43.01	111 133	B_2O_3 WO_3	48	4.34×10^{-4}	4.85×10^{-2}	0.13	98-005-1575 43-1035
	44.85	123	WO_3	38	6.93×10^{-4}	6.03×10^{-2}	0.16	43-1035
	47.55	112 312	B_2O_3 WO_3	39	6.57×10^{-4}	5.97×10^{-2}	0.15	98-005-1575 43-1035
	62.91	143	WO_3	25	1.60×10^{-3}	8.90×10^{-2}	0.17	ICDD 20-1324
	75.89	030	B_2O_3	22	2.07×10^{-3}	1.03×10^{-1}	0.17	98-005-1575

the ionic radii of W^{6+} (0.62Å) and B^{3+} (0.2Å) [1]. Since this large difference between dopant and host atoms, i.e., tungsten and oxygen, the dopant tends to bond with oxygen [15,16] instead of aggregation in the grain boundary or being substituted into the tungsten location inside the WO_3 structure. The emerging B_2O_3 was crystalline, and the origin of the extra peak that emerged in the thin film that was produced is not obviously understandable.

XPS is widely utilized for determining the chemical composition of a surface. The elemental results of the films coated onto both substrates are illustrated in Figure 5. Regarding the patterns, there are W and O peaks in the spectrum. Meanwhile, the resulting patterns have C, N, Si, and B impurities. The Si peak gives rise to the substrate and the C and N are originated from the environment [6]. The doublet peaks in Figure 5a show the W4f valence state in the coated films. Only one state in the films demonstrates the one oxidation state in the tungsten atom. The W4f peak centers emerged at 35.3 eV and 37.4 eV, respectively, identifying this structure's 4f7/2 and 4f5/2 for W^{6+} [7,17]. The absorbance and transmittance of the films upon both substrates are shown in Figure 5 c-f. There are two regions in the absorbance spectrum; the first covers 200-320 nm and 320-1100 nm. There is an electronic transition in the thin film deposited onto the glass substrates for both cases.

The optical band gap (E_g) value of the thin films coated on glass substrates is shown in Figure 6d. The E_g of

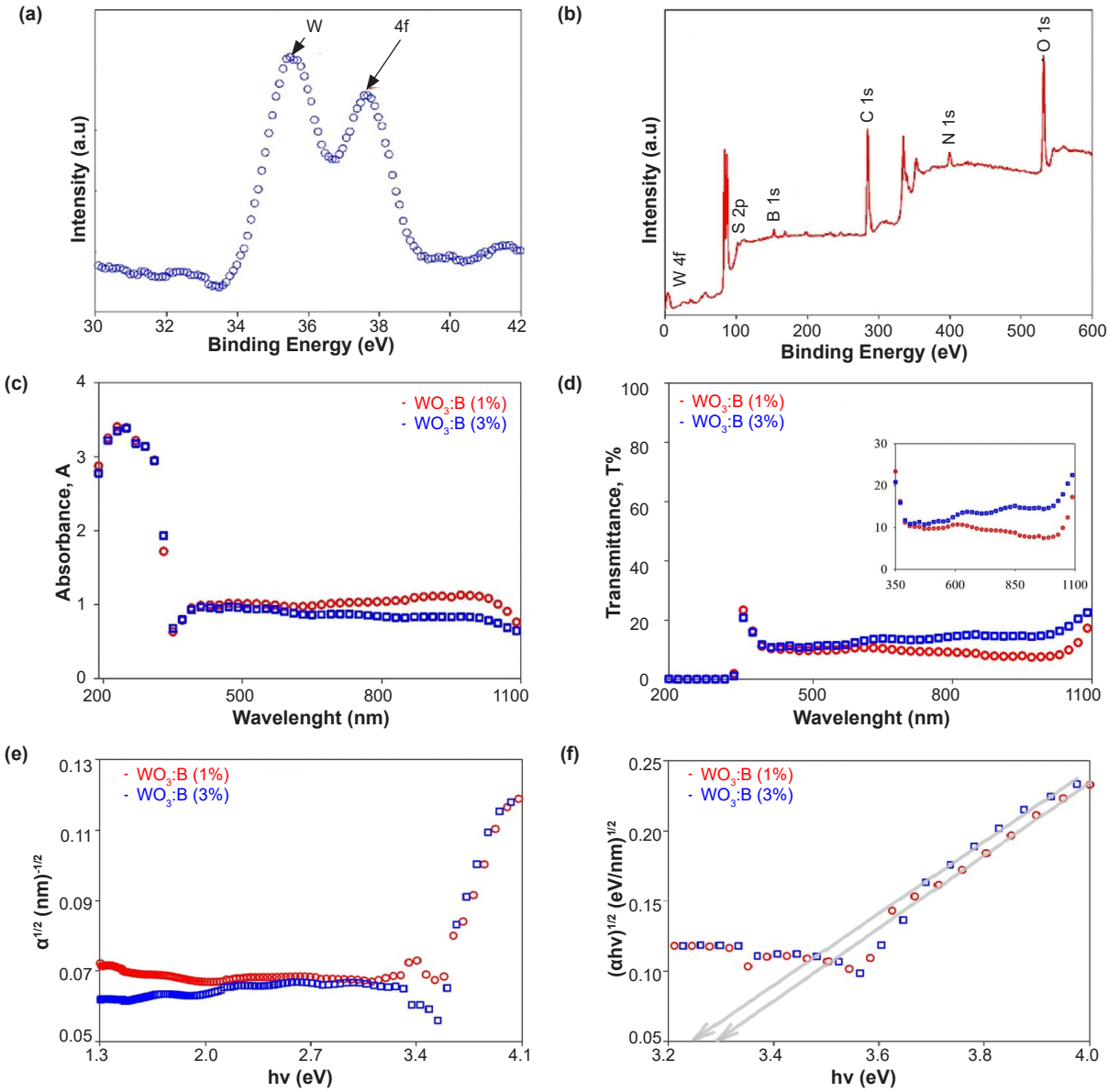

Figure 5. The a) narrow scan of W, and b) wide scan of the coated films. The optical results of the coated boron-doped WO_3 upon glass substrates, c) absorbance, d) transmittance, e) absorption coefficient, and f) optical band gap (E_g).

the thin films is computed using Eq. (5) [18]:

$$(\alpha hv)^n = A\,(hv - E_g) \tag{5}$$

the α, hv, and A are absorption coefficients, photon energy, and a constant. The A is defined as the band-band transition well-known as tailing values. This parameter also presented the coated film quality. In the above formula, the n describes the nature of transition and, in this case, is equal to 2 and 1/2 for direct and indirect optical band gap situations. In the present study, the electronic transition equals ½, which shows the indirect allowed transition of WO_3. The absorption coefficient (α) of the films is calculated by Eq. (6), where T is the transmittance of the coated films, and d is the thickness of films measured by Filmetrics. The E_g values of the WO_3:B films for both 1% and 3% on glass substrates were 3.23 [19] and 3.25 eV [20], respectively.

$$\alpha = \frac{Ln\,(1/T)}{d} \tag{6}$$

The optical parameters such as refraction index (n), reflectance (R), real (ε_{real}), and imaginary ($\varepsilon_{imaginary}$) dielectric constants and optical loss factor (tan δ) of the prepared films on both substrates are illustrated in Figure 6. The parameters show normal distribution in the given wavelength range. The refractive index of the films is in the range of 2.10-2.45. The measured values coincide well with the literature [7,21,22]. The higher refractive index shows a higher packing density and is related to the lower amount of voids and lattice defects [8]. Regardless of the substrate nature, the increase in the dopant value leads to higher packing density.

The real and imaginary parts of dielectric constants and loss function of the films are calculated according to Eq. (7):

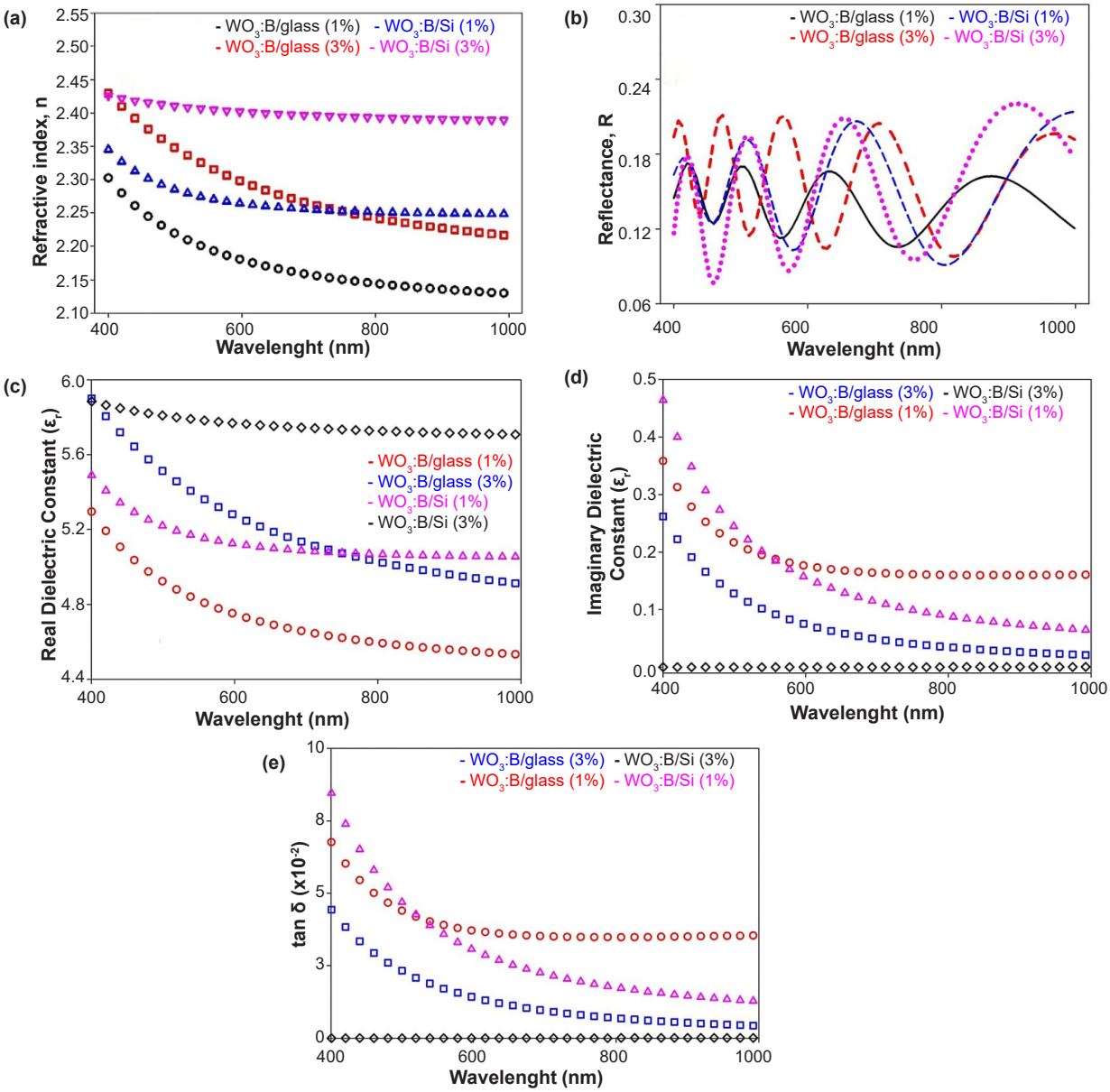

Figure 6. The a) refractive index, b) reflectance, c, d) Real and imaginary dielectric constant, and e) optical loss factor of the films coated onto the glass substrate.

$$\varepsilon(\lambda) = \varepsilon_{real}(\lambda) + \varepsilon_{imaginary}(\lambda) \quad (7)$$

Those are defined in Eq. (8-10):

$$\varepsilon_{real}(\lambda) = n^2 - k^2 \quad (8)$$

$$\varepsilon_{imaginary}(\lambda) = 2nk \quad (9)$$

$$\tan\delta = {}^{\varepsilon_{imaginary}}/_{\varepsilon_{real}} \quad (10)$$

Increasing the wavelength reduces this trend, which causes normal distribution [23]. The optical loss factor of the WO_3:B with different boron dopant amounts is shown minimum value compared to other published reports [19]. The lower optical loss factor originated from lower grain size [24]. This phenomenon is proved by crystallite size computed by the Scherrer equation which may cause a higher conductivity by increasing the amount of crystallite and lowering the defect in the structure [25].

4. Conclusions

In this research, boron-doped WO_3 was successfully coated on the glass and Si substrates using a plasma-based PVD system. Respecting the surface characterization, the roughness of the films directly depends on the boron amount and nature of the substrate. The structural results proved the formation of WO_3 phases on both substrates. An increase in the dopant amount causes a shift in the dominant peak in the XRD patterns. The calculated crystalline sizes for both films confirmed nanometer dimensions ranging from 14 to 49 nm. According to the optical results, the optical band gap (E_g) of the WO_3:B (1%) and WO_3:B (3%) films were obtained as 3.23 and 3.25 eV, respectively. The increase in the boron leads to an increase in the packing density of the films. There is no relationship between the substrate structure nature and packing density. Respecting this research results, there is a direct relationship between crystallite size

and lower optical loss function. The elemental analysis shows the presence of W and O in the spectrum.

5. Acknowledgements

The author would like to thank Kocaeli Health and Technology University for supporting the project (KOSTU BAP 2023/1).

References

[1]. Al-Kuhaili, M. F., & Drmosh, Q. A. (2022). Investigating the structural and optoelectronic properties of co-sputtered Fe-doped WO3 thin films and their suitability for photocatalytic applications. *Materials Chemistry and Physics*, *281*, 125897. https://doi.org/10.1016/j.matchemphys.2022.125897.

[2]. Thakur, A. K., Limaye, M. V., Rakshit, S., Maity, K. N., Gupta, V., Sharma, P. K., & Singh, S. B. (2018). Controlled synthesis of WO3 nanostructures: optical, structural and electrochemical properties. *Materials Research Express*, *6*(2), 025006. https://doi.org/10.1088/2053-1591/aae991.

[3]. Patterson, A. L. (1939). The Scherrer formula for X-ray particle size determination. *Physical Review*, *56*(10), 978. https://doi.org/10.1103/PhysRev.56.978.

[4]. Demirkol, U., Pat, S., Mohammadigharehbagh, R., Musaoğlu, C., Özgür, M., Elmas, S., ... & Korkmaz, Ş. (2019). Determination of the structural, morphological and optical properties of graphene doped SnO thin films deposited by using thermionic vacuum arc technique. *Physica B: Condensed Matter*, *569*, 14-19. https://doi.org/10.1016/j.physb.2019.05.035.

[5]. Ammar, A. U., Stan, M., Popa, A., Toloman, D., Macavei, S., Leostean, C., ... & Rostas, A. M. (2023). All-in-one supercapacitor devices based on nanosized Mn4+-doped WO3. *Journal of Energy Storage*, *72*, 108599. https://doi.org/10.1016/j.est.2023.108599.

[6]. Gupta, D., Chauhan, V., Mahajan, A., Gupta, R., Ali, S. A., & Kumar, R. (2023). Influence of gamma radiation on optical, structural and surface morphological properties of WO3 thin films grown by RF sputtering. *Radiation Physics and Chemistry*, *202*, 110554. https://doi.org/10.1016/j.radphyschem.2022.110554.

[7]. Kavitha, V. S., Krishnan, R. R., Sreedharan, R. S., Suresh, K., Jayasankar, C. K., & Pillai, V. M. (2019). Tb3+-doped WO3 thin films: A potential candidate in white light emitting devices. *Journal of Alloys and Compounds*, *788*, 429-445. https://doi.org/10.1016/j.jallcom.2019.02.222.

[8]. Jain, R. K., & Khanna, A. (2021). CuO-doped WO3 thin film H2S sensors. *Sensors and Actuators B: Chemical*, *343*, 130153. https://doi.org/10.1016/j.snb.2021.130153.

[9]. Reddy G V, A., Kumar, K. N., Sattar, S. A., Shetty, H. D., Prakash, N. G., Jafri, R. I., ... & Ansar, S. (2023). Effect of post annealing on DC magnetron sputtered tungsten oxide (WO3) thin films for smartwindow applications. *Physica B: Condensed Matter*, *664*, 414996. https://doi.org/10.1016/j.physb.2023.414996.

[10]. Elmas, S., Pat, S., Mohammadigharehbagh, R., Musaoğlu, C., Özgür, M., Demirkol, U., ... & Korkmaz, Ş. (2019). Determination of physical properties of graphene doped ZnO (ZnO: Gr) nanocomposite thin films deposited by a thermionic vacuum arc technique. *Physica B: Condensed Matter*, *557*, 27-33. https://doi.org/10.1016/j.physb.2018.12.039.

[11]. Özgür, M., Pat, S., Mohammadigharehbagh, R., Musaoğlu, C., Demirkol, U., Elmas, S., ... & Korkmaz, Ş. (2019). Sn doped ZnO thin film deposition using thermionic vacuum arc technique. *Journal of Alloys and Compounds*, *774*, 1017-1023. https://doi.org/10.1016/j.jallcom.2018.10.020.

[12]. Alsaad, A. M., Al-Bataineh, Q. M., Ahmad, A. A., Albataineh, Z., & Telfah, A. (2020). Optical band gap and refractive index dispersion parameters of boron-doped ZnO thin films: A novel derived mathematical model from the experimental transmission spectra. *Optik*, *211*, 164641. https://doi.org/10.1016/j.ijleo.2020.164641.

[13]. Eskalen, H., Kavun, Y., Kerli, S., & Eken, S. (2020). An investigation of radiation shielding properties of boron doped ZnO thin films. *Optical Materials*, *105*, 109871. https://doi.org/10.1016/j.optmat.2020.109871

[14]. Wong, L. H., & Lai, Y. S. (2021). Substrate temperature dependence of material, optical, and electronic properties of boron-doped ZnO thin films. *Optical Materials*, *115*, 111052. https://doi.org/10.1016/j.optmat.2021.111052.

[15]. Özgür, M., Pat, S., Mohammadigharehbagh, R., Musaoğlu, C., Demirkol, U., Elmas, S., ... & Korkmaz, Ş. (2019). Al doped ZnO thin film deposition by thermionic vacuum arc. *Journal of Materials Science: Materials in Electronics*, *30*, 624-630. https://doi.org/10.1007/s10854-018-0329-x.

[16]. Raja, M., Marnadu, R., Balaji, M., Ravikumar, K., Krishna, V. G., Kumar, M., & Massoud, E. E. S. (2022). Fabrication and characterization of novel Ga-doped WO3 films and n-Ga@ WO3/p-Si junction diode for optoelectronic device applications. *Inorganic Chemistry Communications*, *139*, 109291. https://doi.org/10.1016/j.inoche.2022.109291.

[17]. Mohan, L., Avani, A. V., Kathirvel, P., Marnadu, R., Packiaraj, R., Joshua, J. R., ... & Saravanakumar, S. (2021). Investigation on structural, morphological and electrochemical properties of Mn doped WO3 nanoparticles synthesized by co-precipitation method for supercapacitor applications. *Journal of Alloys and Compounds*, *882*, 160670. https://doi.org/10.1016/j.jallcom.2021.160670.

[18]. Lokhande, B. J., Patil, P. S., & Uplane, M. D. (2001). Studies on structural, optical and electrical properties of boron doped zinc oxide films prepared by spray pyrolysis technique. *Physica B: Condensed Matter*, *302*, 59-63. https://doi.org/10.1016/S0921-4526(01)00405-7.

[19]. Xu, X. G., Yang, H. L., Wu, Y., Zhang, D. L., Wu, S. Z., Miao, J., ... & Wang, B. Y. (2010). Intrinsic room temperature ferromagnetism in boron-doped ZnO. *Applied Physics Letters*, *97*(23) 1-9. https://doi.org/10.1063/1.3524493.

[20]. Thalji, M. R., Ali, G. A., Algarni, H., & Chong, K. F. (2019). Al3+ ion intercalation pseudocapacitance study of W18O49 nanostructure. *Journal of Power Sources*, *438*, 227028. https://doi.org/10.1016/j.jpowsour.2019.227028.

[21]. Tauc, J., Grigorovici, R., & Vancu, A. (1966). Optical properties and electronic structure of amorphous germanium. *Physica Status Solidi (b)*, *15*(2), 627-637. https://doi.org/10.1002/pssb.19660150224.

[22]. Kavitha, V. S., Suresh, S., Chalana, S. R., & Pillai, V. M. (2019). Luminescent Ta doped WO3 thin films as a probable candidate for excitonic solar cell applications. *Applied Surface Science*, *466*, 289-300. https://doi.org/10.1016/j.apsusc.2018.10.007.

[23]. Sriram, S. R., Parne, S. R., Pothukanuri, N., & Edla, D. R. (2023). Synthesis and characterization of pure and Cu-doped WO3 thin films for high performance of toxic gas sensing applications. *Applied Surface Science Advances*, *15*, 100411. https://doi.org/10.1016/j.apsadv.2023.100411.

[24]. Charles, C., Martin, N., Devel, M., Ollitrault, J., & Billard, A. (2013). Correlation between structural and optical properties of WO3 thin films sputter deposited by glancing angle deposition. *Thin Solid Films*, *534*, 275-281. https://doi.org/10.1016/j.tsf.2013.03.004.

[25]. Hutchins, M. G., Abu-Alkhair, O., El-Nahass, M. M., & Abd El-Hady, K. (2006). Structural and optical characterisation of thermally evaporated tungsten trioxide (WO3) thin films. *Materials Chemistry and Physics*, *98*(2-3), 401-405. https://doi.org/10.1016/j.matchemphys.2005.09.052.

[26]. Al-Salami, A. E., Dahshan, A., & Shaaban, E. R. (2017). Effect of film thickness on structural and optical properties of Cd-Zn-Te grown on glass and ITO substrates using electron beam evaporation. *Optik*, *150*, 34-47. https://doi.org/10.1016/j.ijleo.2017.09.062.

[27]. Huang, X., Zhang, H., Lai, Y., & Li, J. (2017). The lowered dielectric loss tangent and grain boundary effects in fluorine-doped calcium copper titanate ceramics. *Applied Physics A*, *123*, 1-7. https://doi.org/10.1007/s00339-017-0947-9.

[28]. Sangwong, N., Somphan, W., Thongbai, P., Yamwong, T., & Meansiri, S. (2012). Electrical responses and dielectric relaxations in giant permittivity NaCu3 Ti3 TaO12 ceramics. *Applied Physics A*, *108*, 385-392. https://doi.org/10.1007/s00339-012-6897-3.